



**HAL**  
open science

## Structural properties of amorphous silicon prepared from hydrogen diluted silane

Miro Zeman, Gijs van Elzaker, Frans D Tichelaar, Pavol Sutta

► **To cite this version:**

Miro Zeman, Gijs van Elzaker, Frans D Tichelaar, Pavol Sutta. Structural properties of amorphous silicon prepared from hydrogen diluted silane. *Philosophical Magazine*, 2009, 89 (28-30), pp.2435-2448. 10.1080/14786430902960137 . hal-00519087

**HAL Id: hal-00519087**

**<https://hal.science/hal-00519087>**

Submitted on 18 Sep 2010

**HAL** is a multi-disciplinary open access archive for the deposit and dissemination of scientific research documents, whether they are published or not. The documents may come from teaching and research institutions in France or abroad, or from public or private research centers.

L'archive ouverte pluridisciplinaire **HAL**, est destinée au dépôt et à la diffusion de documents scientifiques de niveau recherche, publiés ou non, émanant des établissements d'enseignement et de recherche français ou étrangers, des laboratoires publics ou privés.



**Structural properties of amorphous silicon prepared from hydrogen diluted silane**

Journal:	<i>Philosophical Magazine &amp; Philosophical Magazine Letters</i>
Manuscript ID:	TPHM-08-Oct-0356.R1
Journal Selection:	Philosophical Magazine
Date Submitted by the Author:	19-Dec-2008
Complete List of Authors:	Zeman, Miro; Delft University of Technology, Dimes van Elzaker, Gijs; Delft University of Technology, Dimes Tichelaar, Frans; Delft University of Technology, National Centre for HREM Sutta, Pavol; University of West Bohemia, New Technologies - Research Centre
Keywords:	a-Si:H, microcrystalline, thin-film solar cells, XRD
Keywords (user supplied):	structural analysis



## Structural properties of amorphous silicon prepared from hydrogen diluted silane.

M. Zeman<sup>\*1</sup>, G. van Elzaker<sup>1</sup>, F.D. Tichelaar<sup>2</sup>, P. Sutta<sup>3</sup>

<sup>1</sup> Delft University of Technology, Delft Institute of Microsystems and Nanoelectronics (DIMES), Feldmannweg 17, 2628 CT Delft, Netherlands

<sup>2</sup> Delft University of Technology, NCHREM, Lorentzweg 1, 2628 CJ Delft, The Netherlands

<sup>3</sup> University of West Bohemia, New Technologies – Research Centre, Univerzitní 8, 306 14 Plzeň, Czech Republic

### Abstract

A systematic structural analysis of amorphous silicon films prepared from hydrogen diluted silane using plasma enhanced chemical vapor deposition was carried out. Hydrogen dilution of silane during the growth of a-Si:H absorber layers is used to suppress light-induced degradation of a-Si:H solar cells. Transmission electron microscopy (TEM) shows that for higher hydrogen dilution ratios the growth of films becomes strongly inhomogeneous and the transition from amorphous to microcrystalline phase occurs at a smaller thickness. The detailed X-ray diffraction (XRD) analysis of the amorphous films reveals that the strongest peak in the XRD patterns is located around 27.5 deg and corresponds to the signal from the ordered domains of tetragonal silicon hydride and not from cubic silicon crystallites. The full width half maximum (FWHM) of this peak narrows from 5.1 to 4.8 degrees as the ratio of hydrogen to silane flow (R) increases to 20 and does not change significantly for higher hydrogen dilutions. The presence of silicon hydride ordered domains in amorphous films is confirmed by the lattice imaging method applied to the high resolution TEM recordings. The amorphous silicon films fabricated at different hydrogen dilution were applied as absorber layers in single-junction solar cells. The degradation experiment confirms that the cells with absorber layers deposited using hydrogen dilution are more stable to the light exposure. A clear reduction of the degradation is observed when the dilution ratio is increased from R=0 to R=20. The degradation of solar cells with absorber layers prepared at R > 20 is not reduced by further increasing R.

Keywords: hydrogen diluted amorphous silicon, X-ray diffraction, structural analysis, solar cells

\* Corresponding author. T +31-15-2782409, F +31-15-3622163, Email: m.zeman@tudelft.nl

## 1 Introduction

The first amorphous silicon layers were reported in 1965 as films of "silicon from silane" deposited in a radio frequency glow discharge [1]. Ten years later, Walter Spear and Peter LeComber from the Dundee University reported that amorphous silicon had semiconducting properties. They demonstrated that the conductivity of amorphous silicon can be manipulated by several orders of magnitude by adding some phosphine or diborane gas to the glow discharge gas mixture [2]. It was not recognized immediately that hydrogen plays an important role in the newly made amorphous silicon doped films. In fact, amorphous silicon suitable for electronic applications, requiring doping, is an alloy of silicon and hydrogen. Electronic grade amorphous silicon is therefore called hydrogenated amorphous silicon (a-Si:H).

Soon after demonstrating successful doping of a-Si:H it was observed that a-Si:H under light exposure underwent the reversible changes in electronic properties; known as Staebler-Wronski effect (SWE) [3]. This effect is a drawback to many a-Si:H applications and in particular for thin-film silicon solar cells. Today thin-film silicon solar cell technology is emerging as a serious alternative for bulk crystalline silicon technology. Therefore the understanding and suppression of the SWE effect has become more important. The mechanisms governing the degradation and the role of hydrogen are still under debate [4]. Despite the lack of full understanding, there has been some success in reducing the SWE in a-Si:H based solar cells [5,6,7].

Three different ways to grow amorphous silicon that result in a reduction of the SWE degradation have been reported. The first is to grow a-Si:H using plasma enhanced chemical vapor deposition (PECVD) in which the silane source gas is diluted with hydrogen [8]. The level of dilution is expressed by the dilution ratio  $R$ , which is defined as  $R=[H_2]/[SiH_4]$ . The a-Si:H deposited from hydrogen diluted silane is referred to as protocrystalline silicon (pc-Si:H) [9]. This is related to the fact that, under sufficient hydrogen dilution, the growth of Si:H will eventually evolve from the amorphous phase to the microcrystalline phase. The second approach is a so called polymorphous silicon (pm-Si:H) that is also grown from a mixture of silane and hydrogen but under high pressure conditions in the powder regime of the PECVD deposition [10]. A distinct feature of the polymorphous silicon is the presence of the structurally-ordered nanoscale inclusions in the amorphous matrix [11]. The small crystallites are formed in the gas phase and are embedded in the amorphous film. Finally, amorphous silicon grown by hot wire chemical vapor deposition (HWCVD) at elevated substrate temperatures was also found to be more stable than standard a-Si:H [12].

A common structural property of the amorphous silicon films with increased stability is the narrowing of the first scattering peak (FSP) of the X-Ray Diffraction (XRD) patterns. The narrowing of this peak is an indication for an improved medium range order (MRO). The reduction in the full width at half maximum (FWHM) value of the FSP has been observed by Guha et. al. for hydrogen diluted silicon films [13], by Mahan et. al. for high substrate temperature HWCVD a-Si:H [14] and by S. Lebib et. al. [15] for pm-Si:H. On the other hand, there are strong differences in hydrogen content between the films deposited using PECVD and HWCVD. The hydrogen content of PECVD deposited pc-Si:H and pm-Si:H is similar or slightly larger than that of standard a-Si:H [15,16]. However, a-Si:H deposited at high substrate temperatures using HWCVD has a much lower hydrogen concentration [17]. Mahan suggests that small silicon crystallites are present in pc-Si:H and that the majority of the hydrogen is bonded to these crystallites [18]. The remaining amorphous material is depleted

1  
2  
3 of hydrogen and could be similar to the HWCVD material deposited at elevated temperatures.  
4 The existence of H-rich regions at the boundary between crystallites and the amorphous  
5 matrix has also been observed for pm-Si:H [19].  
6  
7

8 In this article we analyze the structural properties of Si:H deposited by PECVD using  
9 hydrogen dilution of the silane source gas in the protocrystalline growth regime. The  
10 experimental details of preparation and characterization of the individual films and complete  
11 solar cells that have been used in this work are described in section 2. The influence of the  
12 addition of hydrogen to the silane source gas on the evolution of structural properties is  
13 demonstrated in subsection 3.1 by using the TEM images of the films. Depending on the level  
14 of hydrogen dilution the evolution includes a phase transition from the amorphous to  
15 microcrystalline phase. In subsection 3.2 we focus on structural properties of pc-Si:H, the  
16 amorphous material below the onset of the mixed amorphous and microcrystalline phase. The  
17 influence of the hydrogen dilution on the XRD patterns of these pc-Si:H films and the  
18 analysis of the XRD patterns is presented in this subsection. In particular we investigate the  
19 narrowing of the FSP in the XRD spectra. The high resolution TEM (HRTEM) images of pc-  
20 Si:H and their analysis is presented in subsection 3.3. In subsection 3.4 the results from  
21 Raman spectroscopy and infrared spectroscopy are presented and discussed. The pc-Si:H  
22 films fabricated at different hydrogen dilutions were applied as absorber layers in single-  
23 junction solar cells. In Section 4 the results of the degradation behavior of these solar cells is  
24 investigated and related to the structural properties of the films.  
25  
26  
27  
28  
29

## 30 2 Experimental details

31  
32 Individual films and solar-cell absorber layers were deposited in the AMOR cluster tool under  
33 the following deposition conditions; an rf-power of 4 W, a silane flow of 5 sccm, a substrate  
34 temperature of 180 °C and a chamber pressure of 2.6 mbar. The hydrogen dilution was varied  
35 between  $R > 0$  and  $R = 40$ . An undiluted  $R = 0$  reference film was grown at an rf-power of 4  
36 W, a pressure of 0.7 mbar, a silane flow of 40 sccm and a substrate temperature of 180 °C.  
37 The thickness of all films was approximately 300 nm, which corresponds to the thickness of  
38 the absorber layer in solar cells. The individual films were deposited on Corning Eagle 2000  
39 type glass substrates and c-Si substrates coated with a 20 nm thick a-Si:H layer grown from  
40 pure silane. Single junction p-i-n solar cells were deposited on Asahi U-type substrates using  
41 the above described films as the absorber layers. The solar cells have the following structure:  
42 p-type a-SiC:H layer (10 nm)/a-SiC:H buffer layer/intrinsic absorber layer (300 nm)/n-type a-  
43 Si:H layer (20 nm). The back contact consists of 100 nm silver and 200 nm aluminum.  
44  
45  
46  
47

48 The structural properties of the films were studied by X-ray diffraction analysis using  
49 an automatic powder diffractometer X'pert Pro with a thin film attachment (parallel beam,  
50 asymmetric geometry, fixed incident angle  $\omega$ , 2 $\theta$ -scan) and a proportional detector. Copper  
51  $K\alpha$  characteristic radiation ( $\lambda = 0.154178$  nm) was used. Because the films were around 300  
52 nm thick and the penetration of  $CuK\alpha$  X-rays into the silicon is much more than this value,  
53 the XRD patterns were recorded using an asymmetric geometry in order to keep the volume  
54 of material that is probed constant. The angle of incidence was fixed to 0.5 deg and the  
55 detector moved with a constant step of 0.05 deg from 10 to 65 deg on the 2 $\theta$  scale. The  
56 counting time was 20 seconds per step and the irradiated area of the sample was 15×15 mm<sup>2</sup>.  
57 Due to the asymmetric geometry of the experiment with a fixed incident X-ray beam, the  
58 lattice planes, for which the Bragg condition is fulfilled, are not parallel to the sample surface,  
59 but they are declined to the sample surface about  $\vartheta - \omega$  degrees. The initial processing of the  
60

XRD patterns that includes background determination and subtraction was done using the X'pert HighScore plus software. We used a procedure utilizing the integral breadth of a diffraction line for determining the average size of the ordered domains and micro-strains. This procedure is based on a Voigt function applied to the breadths of the diffraction line as proposed by Langford [20, 21]. Eq. (1) defines the integral breadth,  $\beta$ , and includes two parameters namely the height,  $I_0$ , and the integrated intensity,  $I_{\text{int}}$ , of the diffraction line.

$$\beta = \frac{I_{\text{int}}}{I_0} \quad (1)$$

This procedure can only be used for symmetric line profiles. The measured FSP of the pc-Si:H samples was not symmetric and therefore, prior to the line profile analysis, it was fitted using the least squares method with two symmetric Pearson VII functions. The instrumental resolution of the equipment was taken into account in order to obtain the physical component of the broadening of the diffraction line. The reference measurement of the alumina powder from NIST (National Institute for Standards and Technology) was used for this correction. The physical component of the integral breadth of the diffraction line was then de-convoluted into a Cauchy part,  $\beta_C^f$ , and a Gaussian part  $\beta_G^f$ , which represent the size of the diffracting domains and the micro-strains, respectively. The average size of the ordered domains and micro-strains were determined using Eqs. 2 and 3, respectively [22, 23]:

$$\langle D \rangle = \frac{\lambda}{\beta_C^f \cos(\theta)}, \quad (2)$$

where  $\langle D \rangle$  is the average domain size in the direction perpendicular to the diffracting lattice planes,  $\lambda$  is the x-ray wavelength and  $\theta$  is the Bragg's angle.

$$\langle \varepsilon \rangle = \frac{\beta_G^f}{4 \tan(\theta)}, \quad (3)$$

where  $\langle \varepsilon \rangle$  is the average micro-strain in the diffracting volume.

Cross sectional specimens for TEM were prepared by gluing a protective glass on top of the deposited layers, cutting slices from the stack, and subsequent ion milling to electron transparency. Bright field images and selected area diffraction patterns were taken with a CM30T and CM30UT-FEG Philips TEM operating at 300 kV.

UV-Vis spectra have been taken by a Specord 210 spectrophotometer. Reflectance measurements at nearly normal incidence were carried out with an aluminum sample as a reference, and were used to calculate the film band gap.

Raman spectroscopy measurements were taken using a Renishaw inVia type spectrometer. A laser wavelength of 514 nm was used. Due to the absorption in the a-Si:H this means that approximately 50 nm of the top of the films is probed. The Raman spectra were fitted with Gaussian distribution positioned at the LA (longitudinal acoustic, centred around  $330 \text{ cm}^{-1}$ ), LO (longitudinal optic,  $440 \text{ cm}^{-1}$ ) and TO (transverse optic,  $480 \text{ cm}^{-1}$ ) peaks.

Fourier transform infrared spectroscopy (FTIR) was carried out in transmission mode using a Thermo electron Nicolet 5700 spectrometer. The IR transmission spectrum was

corrected for the substrate absorption, measured prior to the film deposition. The hydrogen content of the films was determined by integrating the absorption peak located between 630  $\text{cm}^{-1}$  to 640  $\text{cm}^{-1}$ . The microstructure parameter  $R^*$  was determined by integrating and comparing the 2000  $\text{cm}^{-1}$  and 2100  $\text{cm}^{-1}$  absorption peaks, which are assigned to the low stretching mode (LSM) of isolated Si-H bonds and the high stretching mode (HSM) of Si-H bonds at internal surfaces such as voids, dihydride, and trihydride bonds, respectively.

The solar cells were degraded with halogen lamps using a power density of  $100\text{mW}/\text{cm}^2$  while they were kept at a constant temperature of 50 °C. The solar cells were characterized by *IV* measurements under standard AM 1.5 illumination conditions.

### 3 Results and discussion

#### 3.1 Structural phase transition

Figure 1 shows TEM images of 1  $\mu\text{m}$  thick films that have been deposited under different hydrogen dilutions on glass [24]. It clearly demonstrates that the growth of silicon films in the protocrystalline growth regime is inhomogeneous for larger dilution ratios ( $R > 20$ ), for which the transition from amorphous to microcrystalline phase can be observed. It confirms the findings from real time spectroscopic ellipsometry measurements [25] that the thickness at which the phase transition occurs depends on the hydrogen dilution and that the transition becomes more abrupt with increasing hydrogen dilution. The transition between different phases of film silicon has recently been explained using the cone kinetics model, based on the different growth rates of the microcrystalline and amorphous phases [26]. Figure 1 demonstrates that in order to properly analyze the dependence of the properties of protocrystalline silicon on  $R$ , the deposition conditions have to be chosen very carefully. The deposition conditions need to be such that they allow the growth of amorphous films with sufficient thickness over a wide range of  $R$  without crossing the phase transition. Using Raman spectroscopy we verified that the deposition conditions described in section 2 have resulted in 300 nm thick amorphous films for the full range of dilution ratios (up to  $R = 40$ ). (The films shown in Figure 1 were deposited using different conditions [24], and are shown here only to illustrate the effect of  $R$  on the phase transition.)

#### 3.2 Analysis of structural properties with XRD

In this subsection the XRD analysis of the series of pc-Si:H films is presented. Figure 2 shows an example of a measured XRD pattern for the amorphous Si:H film deposited at  $R = 20$ . The sharp peaks on the black line belong to the Laue diffraction from the c-Si substrate created by the continuous X-ray radiation, which was not fully attenuated by the beta filter. Figure 3 shows the FSP, corrected for the background, of the film deposited at  $R = 20$  and the fit of the data with two Pearson VII functions. It was found that the FSP peak of all films of the dilution series could be fitted with a large area peak centered around 27.5 degrees and a smaller peak centered around 32.5 degrees. In Figure 3 the XRD patterns for crystalline silicon (Si) and crystalline silicon hydride ( $\text{Si}_4\text{H}$ ) standards are included. These XRD standards were constructed from the ICDD PDF 2 data file (ICDD – International Centre for Diffraction Data, PDF – powder diffraction file). Comparing these standards to the measured XRD patterns we find a striking match between the position of the two Pearson VII functions and the silicon hydride lines, while the silicon (111) line clearly does not correspond to the center position at

1  
2  
3 27.5 degrees. Given the controversy regarding the origin of the a-Si:H FSP [27], this result  
4 provides an interesting new interpretation of the ordered domains in the amorphous matrix. A  
5 good agreement between the position of the peaks of the measured lines and the standard  
6 XRD patterns of the silicon hydride gives evidence that the diffracting signal comes mainly  
7 from the ordered domains of a tetragonal silicon-hydride [28] and not from ordered domains  
8 of silicon.  
9

10  
11 For comparison, the FSP peak of the XRD pattern measured on a Si:H film containing  
12 the mixed amorphous/microcrystalline phases is shown in Figure 4. This film was deposited  
13 on a glass substrate at  $R = 40$ . **The use of a different substrate has resulted in a different**  
14 **microstructure of the film.** The Raman spectrum confirmed the presence of a crystalline  
15 fraction in the film. The fit of the FSP contains contributions from both the silicon hydride  
16 (001) line and silicon (111) line. The contribution from the silicon hydride (110) line is  
17 suppressed by the signal from the glass substrate. The contribution from silicon crystallites to  
18 the XRD pattern was reported for Si:H films having a mixed amorphous/microcrystalline  
19 phases [27].  
20  
21  
22

23  
24 For all films, the  $2\theta$  positions of the strongest peak in our XRD patterns,  
25 corresponding to the silicon hydride (001) line in Figure 3, are between 27.49 and 27.59 deg.  
26 These positions result in inter-planar spacings of 0.3245 to 0.3233 nm. For the tetragonal  
27 silicon hydride lattice the reference values of the  $2\theta$  peak position and inter-planar spacing of  
28 the (001) line are 27.53 deg and 0.3238 nm, respectively [28]. The results from our  
29 measurements match well with the reference values of the (001) line of silicon hydride lattice.  
30 The lattice spacings represent distances between the lattice planes occupied mostly by silicon  
31 atoms. Hydrogen atoms, when they are incorporated in the lattice structure (for example as  
32 hydrides), can influence the lattice parameters of the structure and cause the observed  
33 deviations.  
34  
35

36  
37 The dominant peak at 27.5 degrees was used for the further analysis of the structural  
38 properties. Figure 5 shows the FWHM values of this peak as a function of the hydrogen  
39 dilution. The figure demonstrates that the FWHM decreases with increasing  $R$  from 0 to 20,  
40 and remains nearly constant when  $R$  is further increased from  $R = 20$  to  $R = 40$ . This confirms  
41 previous reports about the narrowing of the FSP [13], but shows for the first time that this  
42 effect saturates for a certain value of  $R$ . The resulting values for the domain size and micro-  
43 strains are presented in Table 1. The domain size increases slightly with  $R$ , and the micro-  
44 strain is nearly independent of  $R$ . The values around 0.09 for the micro-strain are high which  
45 points out that the structure is locally strongly disordered and the majority of the  
46 investigated specimen volume is strained. Information about the dimensions of coherently  
47 diffracting domains (crystallites) is only a rough estimation and can vary from sample to  
48 sample depending on the initial interfacial conditions during the film deposition.  
49  
50

### 51 52 **3.3 HRTEM analysis**

53  
54 Figure 6 shows the HRTEM recording of the pc-Si:H film prepared at  $R = 40$ . The images do  
55 not show clear and closed crystalline formations as is the case of polymorphous silicon films  
56 [11]. However, the atomic structure has definitely some degree of ordering represented by  
57 many small areas in the order of less than 3 nm of atoms forming parallel planes. Analyzing  
58 the ordered region indicated in Figure 6 by the lattice imaging method the inter-planar  
59 spacings are determined to be  $3.4 \pm 0.1$  nm. This matches well with the (001) orientation of the  
60 silicon hydride lattice.

### 3.4 Raman, infrared absorption and optical spectroscopy

The Raman spectra revealed a clear trend in the TO peak position with increasing hydrogen dilution during the deposition of films. Figure 7 demonstrates that with the increasing R the peak shifts from  $483\text{ cm}^{-1}$  to  $486\text{ cm}^{-1}$ . A similar observation is reported by Tsu et. al., who attributed this shift to the presence of regions with increased structural order [29]. However, the position of the TO peak does not change significantly for the films deposited at  $R > 20$ . This result is in agreement with the trend of narrowing and saturation of the HWFM the FSP of the XRD patterns and suggests that when the ordering of film structure achieves an optimal state, increased hydrogen dilution during the growth does not improve it, but results in accelerated phase transition. The FWHM width of the TO peak does not change significantly with hydrogen dilution and has a value of approximately  $59\text{ cm}^{-1}$  for all films.

The hydrogen content increased from 8 at.% to more than 16 at.% in films deposited at  $R=5$  and  $R=40$ , respectively. The trend of increasing hydrogen content in the pc-Si:H films prepared at higher R has been observed also by other groups [16]. The position of  $630\text{ cm}^{-1}$  peak was used to evaluate bonding of hydrogen to crystalline silicon grains in the films [18]. Figure 7 shows that there is no obvious trend in the peak position in films deposited at different R; the peak position lies between  $633\text{ cm}^{-1}$  and  $637\text{ cm}^{-1}$ . In correspondence to our findings from the XRD and HRTEM, the analysis of the peak position does not reveal the presence of silicon crystallites in pc-Si:H films as the shift of the peak towards  $620\text{ cm}^{-1}$  is not observed [18]. Figure 8 shows an example of the Si-H stretching mode absorption peaks in the range of  $2000 - 2200\text{ cm}^{-1}$  for the pc-Si:H film deposited at  $R = 20$ . The figure demonstrates that the absorption in the film is predominantly by the LSM at  $2000\text{ cm}^{-1}$  resulting in a low microstructure parameter  $R^*$ . The microstructure parameter for all films is presented in Table 1.  $R^*$  increases with increasing hydrogen dilution from less than 1% for the film deposited at  $R = 5$  to almost 4% and for  $R = 40$ . The  $R^*$  is widely used to characterize the microstructure in the a-Si:H network and the very low value of  $R^*$  for diluted films indicates a dense network.

The photon energy at which the absorption coefficient of films is equal to  $10^4\text{ cm}^{-1}$  ( $E_{04}$ ) was used as a measure for the optical band gap of the films. The band gap of the films is presented in Table 1. With the increasing R the band gap increases from 1.87 eV ( $R = 5$ ) to 2.09 eV ( $R = 40$ ). The increasing bandgap is a result of the improved structural order and the increasing hydrogen concentration in the films [30].

### 4 Degradation of solar cell with pc-Si:H absorber layers

The a-Si:H films prepared from hydrogen diluted silane were implemented as absorber layers in p-i-n solar cells. The absorber layers were deposited at equal deposition conditions as the individual films using hydrogen dilutions  $R = 0, 10, 20, 30, 40$ . The solar cells were subjected to a degradation experiment. Figure 9 shows the evolution of the efficiency of the solar cells with exposure time. Figure 10 shows the change in the fill factor. In both figures the parameters are normalized to their initial values before degradation. The degradation experiment confirms that the cells with absorber layers deposited using hydrogen dilution are more stable to the light exposure. A clear reduction of the degradation is observed when the dilution ratio is already increased from  $R = 0$  to  $R = 10$  and the degradation is further suppressed when R is increased to 20. However, solar cells with the absorber layers prepared

1  
2  
3 at  $R > 20$  exhibit similar degradation behavior as the cell with the absorber layer prepared at  
4  $R = 20$ . The efficiency of the solar cells with the absorber layers prepared at  $R \geq 20$  stabilizes  
5 around 88% of their initial efficiency.  
6  
7

8 The similar degradation behavior of solar cells with the absorber layers deposited at  $R$   
9  $\geq 20$  indicates that there is a correlation with structural properties observed for the individual  
10 films. The saturation of the FWHM value of the FSP and stabilization of the TO peak in the  
11 Raman spectra for pc-Si:H films prepared at  $R \geq 20$  is a strong indication that the structural  
12 order has achieved an optimal state in these films. The presence of small ordered domains of  
13 silicon hydride contributes to the observed medium range order in the films. The increased  
14 hydrogen dilution does not improve the ordering but accelerates the amorphous/  
15 microcrystalline phase transition. The improved structural order contributes to suppressing the  
16 light induced degradation by decreasing the amount of weak Si-Si bonds which are removed  
17 by hydrogen etching of the growing surface [31]. However, the improved structural order in  
18 amorphous films still does not prevent the occurrence of the degradation. The mechanisms  
19 that initiate the degradation have to be further investigated in order to fully prevent it.  
20  
21  
22  
23  
24  
25  
26  
27  
28  
29  
30  
31  
32  
33  
34  
35  
36  
37  
38  
39  
40  
41  
42  
43  
44  
45  
46  
47  
48  
49  
50  
51  
52  
53  
54  
55  
56  
57  
58  
59  
60

## 5 Conclusions

Dilution of the silane source gas with hydrogen during the PECVD deposition of silicon films results in interesting modifications of the structural properties of the films in reference to undiluted ones. The most pronounced effect is the transition from amorphous to the microcrystalline phase, which, depending on the amount of hydrogen dilution, occurs at a certain threshold thickness. The presented TEM images visualize the inhomogeneous growth and the phase transition and they are in agreement with phase diagrams that were obtained from real-time in situ ellipsometry.

Although the phase transition is the most evident effect of the hydrogen dilution, more subtle changes do also occur in the amorphous silicon that is grown below the threshold thickness before the phase transition. The XRD analysis of the amorphous films revealed the narrowing of the FSP of the XRD patterns with increasing hydrogen dilution. For the first time it is demonstrated that this effect saturates and an increase of the hydrogen dilution above a certain value does not result in a further narrowing of the FSP. However, the most important result from the XRD analysis of the hydrogen diluted amorphous silicon films is the presence of ordered domains of tetragonal silicon hydride in the films. The XRD pattern is obtained from diffracting domains of tetragonal silicon hydride and not from cubic silicon. This conclusion is also confirmed from the lattice imaging method applied to HRTEM images of the films.

The shift and stabilization of the TO peak in the Raman spectra of the films towards a higher wavenumber with increasing hydrogen dilution confirms an increased structural order. The low microstructure parameter ( $R^* < 4\%$ ) determined from the analysis of the IR absorption spectra is an indication for structurally dense films.

To test the improved stability of the hydrogen diluted a-Si:H films against light exposure solar cells were fabricated in which the films were implemented as the absorber layer. A degradation experiment demonstrated the improved stability of the cells with absorber layers prepared at higher hydrogen dilution. However, the degradation of solar cells with the absorber layers prepared at  $R > 20$  is not reduced by increasing  $R$ . This result indicates that there is a strong link between the medium range order, represented by the saturation of the narrowing of the FSP width of the XRD pattern in the films prepared at  $R > 20$ , and the degradation behavior of the solar cells.

## Acknowledgements

This work was supported by Delft University of Technology as a part of the SENECU project and partially funded through the project of Ministry of Education, Sports and Youth of the Czech Republic No. 1M06031.

## References

- [1] H.F. Sterling and R.C.G. Swann, *Solid-State Electron.* 8 (8), 653 (1965).
- [2] W.E. Spear and P.G. Le Comber, *Solid State Communications* 17 (9), 1193 (1975).
- [3] D.L. Staebler and C.R. Wronski, *Appl. Phys. Lett.* 31, 292 (1977).
- [4] H. Fritzsche, *Annu. Rev. Mater. Res.*, 31 (2001) 47.
- [5] Shimizu, A. Matsuda, M. Kondo, *Solar Energy Materials & Solar Cells* 92, 1241 (2008)
- [6] N. Wang, V.L. Dalal, *Journal of Non-Crystalline Solids* 352, 1937 (2006)
- [7] W.Du, X. Liao, X. Cao et al., *Journal of Non-Crystalline Solids* 354, 2155 (2008)
- [8] S. Guha, K.L. Narasimhan, and S.M. Pietruszko, *J. Appl. Phys.* 52 (1981) 859.
- [9] J. Koh, Y. Lee, H. Fujiwara, C.R. Wronsky, R.W. Collins, *App. Phys. Lett.* 73 (1998) 1526.
- [10] R. Butte, R. Meaudre, M. Meaudre et al., *Philosophical Magazine Part B* 79 (7), 1079 (1999).
- [11] P. Roca i Cabarrocas, A. Fontcuberta i Morral, Y. Poissant, *Thin Solid Films* 403 – 404 (2002) 39–46.
- [12] A.H. Mahan, and M. Vanecek, *AIP Conf. Proc.* 234, 195 (1991).
- [13] S. Guha, J. Yang, D.L. Williamson et al., *Applied Physics Letters* 74 (13), 1860 (1999).
- [14] A.H. Mahan, D.L. Williamson, T.E. Furtak, *Mat. Res. Soc. Symp. Proc.* 467 (1997) 657.
- [15] S. Lebib and P. Roca i Cabarrocas, *The European Physical Journal Applied Physics* 26, 17 (2004).
- [16] U. Kroll, J. Meier, A. Shah et al., *J. Appl. Phys.* 80 (9), 4971 (1996).
- [17] A.H. Mahan, J. Carapella, B. P. Nelson et al., *J. Appl. Phys.* 69 (9), 6728 (1991).
- [18] A.H. Mahan, J. Yang, S. Guha, D.L. Williamson, *Phys. Rev. B* 61 (3), 1677 (2000).
- [19] S. Vignoli, Butt, R. et al., *Journal of Physics: Condensed Matter* 15 (43), 7185 (2003).
- [20] J.I. Langford: *J. Appl. Cryst.* (1978) 11, 10-14.
- [21] J.I. Langford, A. Boultif, J.P. Auffrédic and D. Louër: *J. Appl. Cryst.* (1993) 26, 22-33.
- [22] R. Delhez, Th. H. de Keijser, and E. J. Mittemeijer: *Fresenius Z Anal Chem* (1982) 312, 1-16.
- [23] R. Delhez, Th.H. de Keijser, and E.J. Mittemeijer: *Surface Engineering* (1987) Vol. 3, No. 4, 331-342
- [24] G. van Elzaker, V. Nádaždy, F.D. Tichelaar, J.W. Metselaar, and M. Zeman, *Thin Solid Films*, 511 (2006) 252-257.
- [25] R.W. Collins, J. Koh, A.S. Ferlauto, P.I. Rovira, Y. Lee, R.J. Koval, and C.R. Wronski, *Thin Solid Films*, 364 (2000) 129.
- [26] Charles W. Teplin, C. S. Jiang, Paul Stradins et al., *Applied Physics Letters* 92 (9), 093114 (2008).
- [27] D.L. Williamson, *Mater. Res. Soc. Symp. Proc.* 559 (1999) 251.
- [28] S. Minomura, K. Tsuji, H. Oyanagi, and Y. Fujii: *Journal of Non-Crystalline Solids* 35&36 (1980) 513-518.
- [29] D.V. Tsu, B.S. Chao, S.R. Ovshinsky, S.J. Jones, J. Yang, S. Guha, R. Tsu, *Phys. Rev. B* 63 (2001) 125338.
- [30] A.H. Mahan, R. Biswas, L.M. Gedvilas, D.L. Williamson, B.C. Pan, *J. Appl. Phys.* 96 (7), 3818 (2004).
- [31] C. C. Tsai, G. B. Anderson, R. Thompson et al., *Journal of Non-Crystalline Solids* **114** (Part 1), 151 (1989).

1  
2  
3  
4  
5  
6  
7  
8  
9  
10  
11  
12  
13  
14  
15  
16  
17  
18  
19  
20  
21  
22  
23  
24  
25  
26  
27  
28  
29  
30  
31  
32  
33  
34  
35  
36  
37  
38  
39  
40  
41  
42  
43  
44  
45  
46  
47  
48  
49  
50  
51  
52  
53  
54  
55  
56  
57  
58  
59  
60

## Tables

Table 1: Properties of the deposited films deposited at different values of hydrogen dilution R. Deposition rate  $r_d$ , bandgap  $E_{04}$ , hydrogen content  $C_H$ , microstructure parameter  $R^*$ , the FWHM value of the XRD first scattering peak, domain size D and micro-strain  $\epsilon$ .

R	$r_d$ $\text{\AA}/s$	$E_{04}$ eV	$C_H$ at. %	$R^*$ -	FWHM degrees	D nm	$\epsilon$ -
0	2	1.91	10.7	0.029	5.02	6	0.086
5	1.3	1.87	8.6	0.006	4.98	6	0.081
10	1.1	1.89	10.6	0.003	4.92	7	0.087
15	0.8	1.92	12.0	0.010	4.88	6	0.086
20	0.7	1.91	14.0	0.008	4.79	11	0.088
25	0.6	1.9	14.8	0.012	4.81	6	0.089
30	0.5	1.95	14.9	0.018	4.80	7	0.083
35	0.5	1.95	15.6	0.022	4.81	11	0.085
40	0.4	2.09	16.7	0.038	4.80	5	0.079

### Figure captions

Figure 1: Bright field TEM images of a series of 1  $\mu\text{m}$  thick films deposited at increasing hydrogen dilution ratios from  $R=0$  to 40.

Figure 2: Raw XRD patterns measured on a 300 nm thick film deposited with  $R=20$  on a c-Si substrate.

Figure 3: XRD patterns of the FSP after background correction. The peak is fitted with two Pearson VII profiles. Also shown are the XRD lines for crystalline Si and  $\text{Si}_4\text{H}$ .

Figure 4: XRD patterns of the FSP after background correction for Si:H film deposited with  $R = 40$  on a glass substrate. Also shown are the XRD lines for crystalline Si and  $\text{Si}_4\text{H}$ .

Figure 5: FWHM values of the FSP as a function of  $R$ .

Figure 6: HRTEM image of a-Si:H film deposited at  $R = 40$ .

Figure 7: Position of the Raman TO peak and the FTIR  $630\text{ cm}^{-1}$  peak as a function of  $R$ .

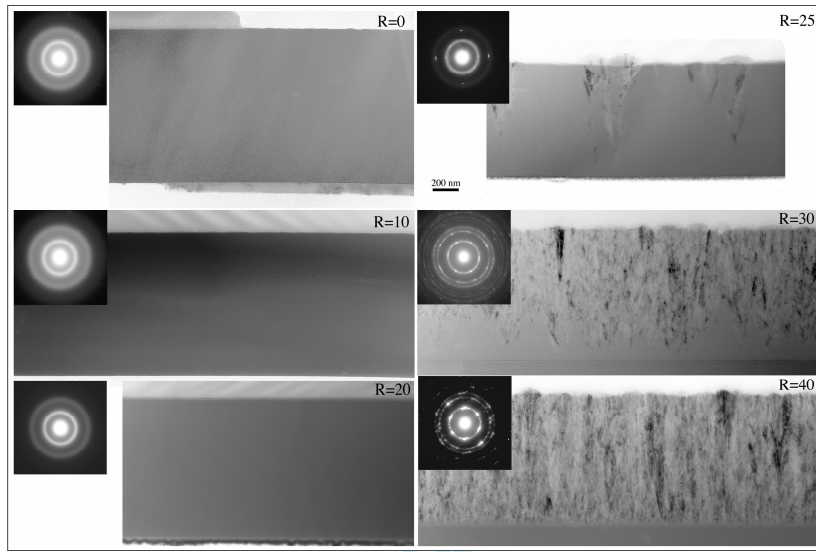
Figure 8: The Si-H stretching mode absorption in the film deposited at  $R = 20$  and the fits around.

Figure 9: Degradation of the efficiency of solar cells in which the absorber layers have been grown at different  $R$ . The data is normalized to the initial efficiency.

Figure 10: Degradation of the fill factor of solar cells in which the absorber layers have been grown at different  $R$ . The data is normalized to the initial fill factor.

Figures

Figure 1:



Peer Review Only

Figure 2:

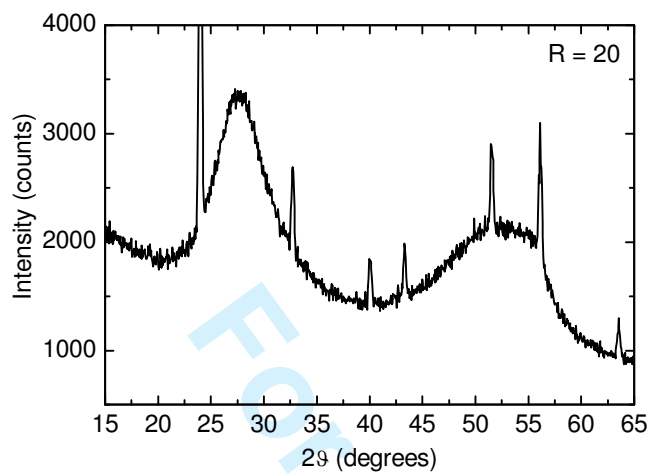


Figure 3:

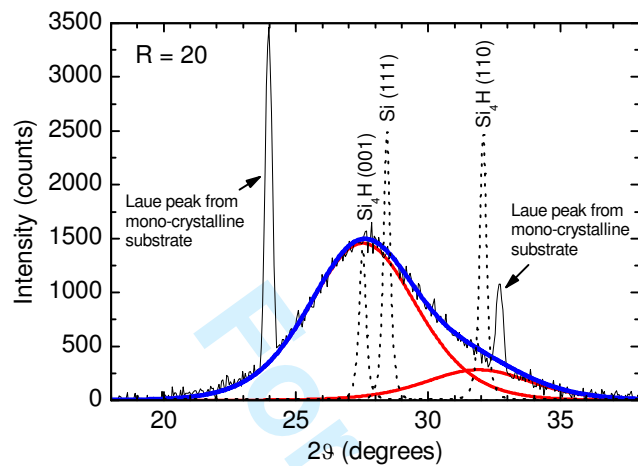
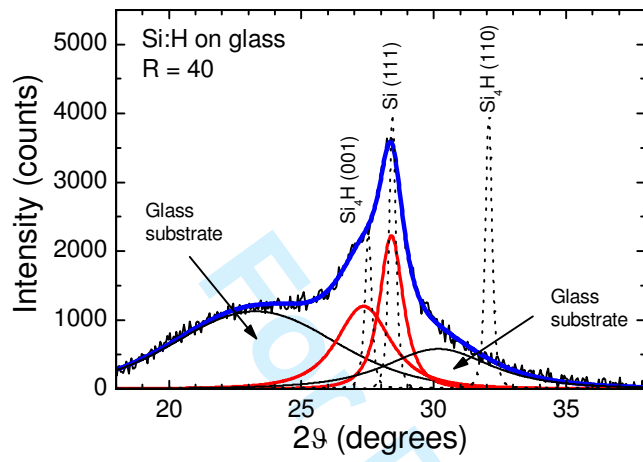


Figure 4:



1  
2  
3  
4  
5  
6  
7  
8  
9  
10  
11  
12  
13  
14  
15  
16  
17  
18  
19  
20  
21  
22  
23  
24  
25  
26  
27  
28  
29  
30  
31  
32  
33  
34  
35  
36  
37  
38  
39  
40  
41  
42  
43  
44  
45  
46  
47  
48  
49  
50  
51  
52  
53  
54  
55  
56  
57  
58  
59  
60

Figure 5:

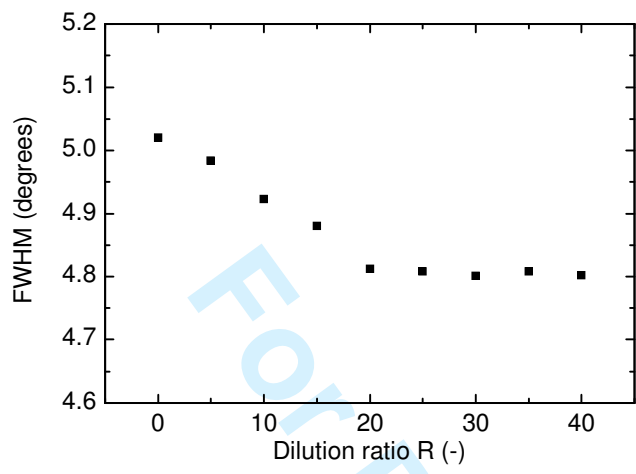
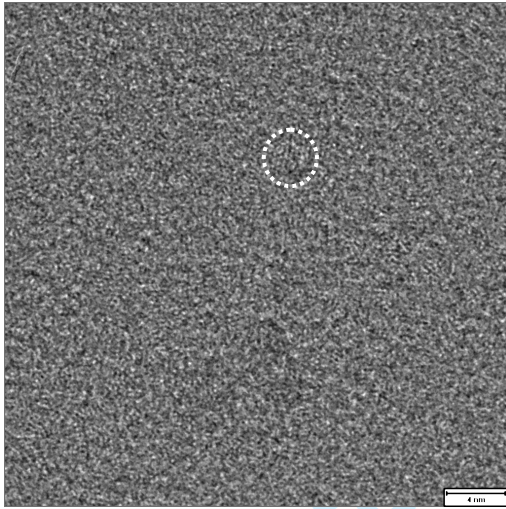


Figure 6:



Peer Review Only

Figure 7

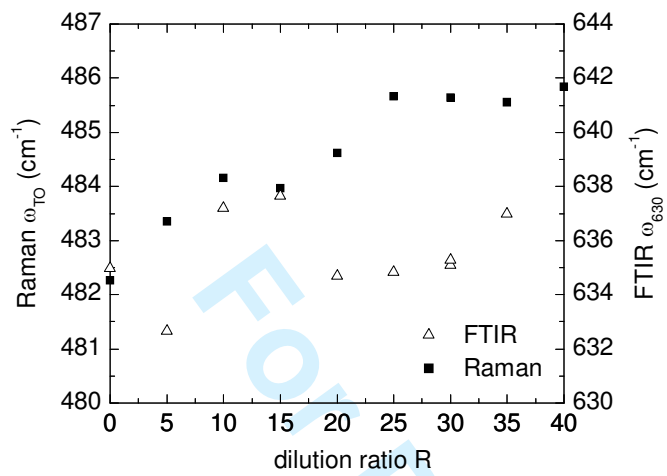
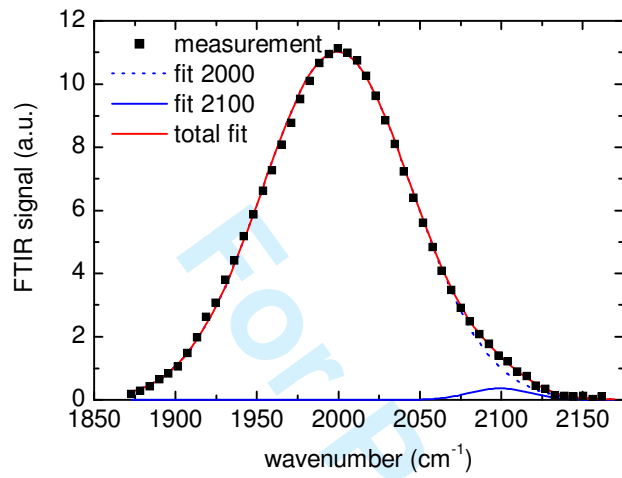


Figure 8



1  
2  
3  
4  
5  
6  
7  
8  
9  
10  
11  
12  
13  
14  
15  
16  
17  
18  
19  
20  
21  
22  
23  
24  
25  
26  
27  
28  
29  
30  
31  
32  
33  
34  
35  
36  
37  
38  
39  
40  
41  
42  
43  
44  
45  
46  
47  
48  
49  
50  
51  
52  
53  
54  
55  
56  
57  
58  
59  
60

Figure 9:

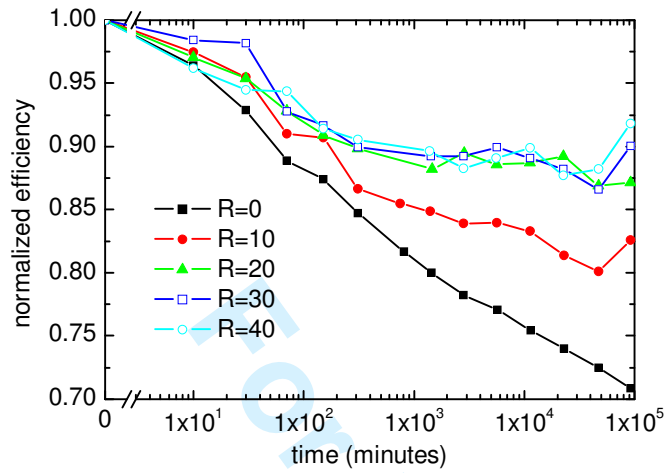
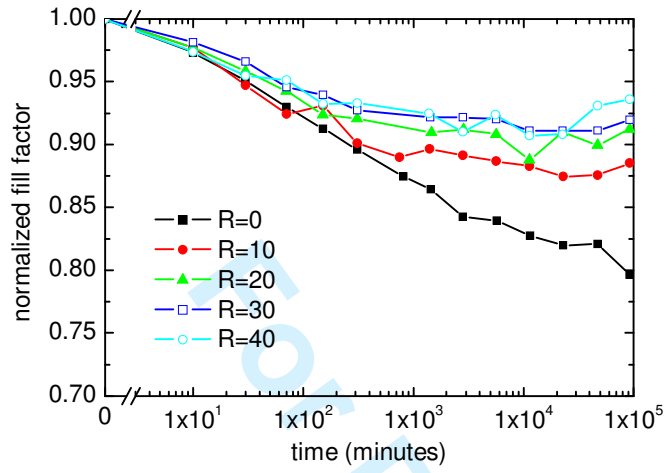


Figure 10:



Peer Review Only

1  
2  
3  
4  
5  
6  
7  
8  
9  
10  
11  
12  
13  
14  
15  
16  
17  
18  
19  
20  
21  
22  
23  
24  
25  
26  
27  
28  
29  
30  
31  
32  
33  
34  
35  
36  
37  
38  
39  
40  
41  
42  
43  
44  
45  
46  
47  
48  
49  
50  
51  
52  
53  
54  
55  
56  
57  
58  
59  
60

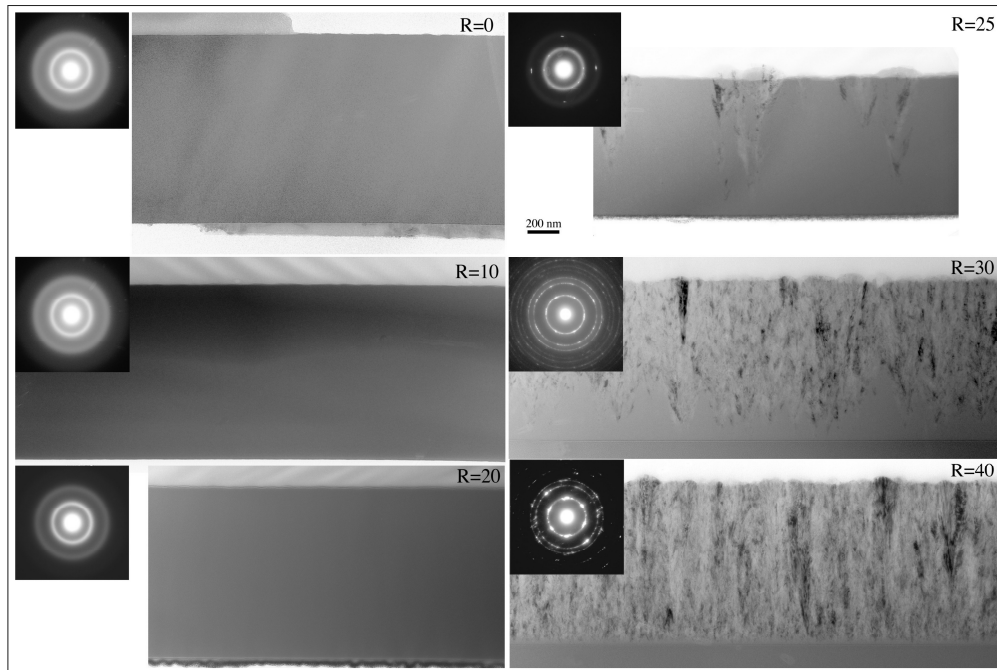


Figure 1: Bright field TEM images of a series of 1  $\mu\text{m}$  thick films deposited at increasing hydrogen dilution ratios from R=0 to 40.

Review Only

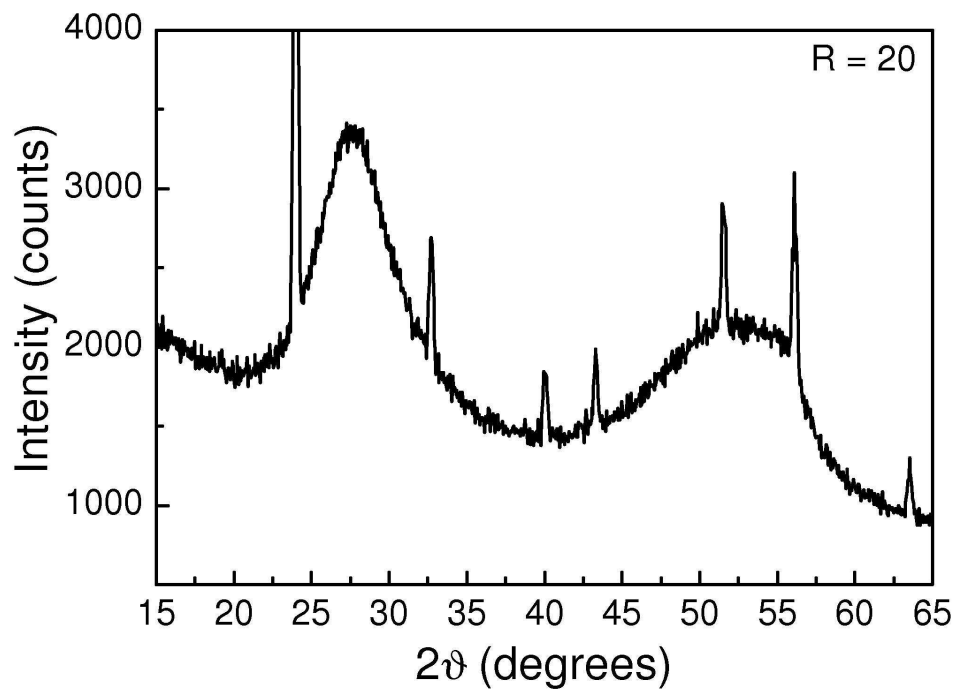
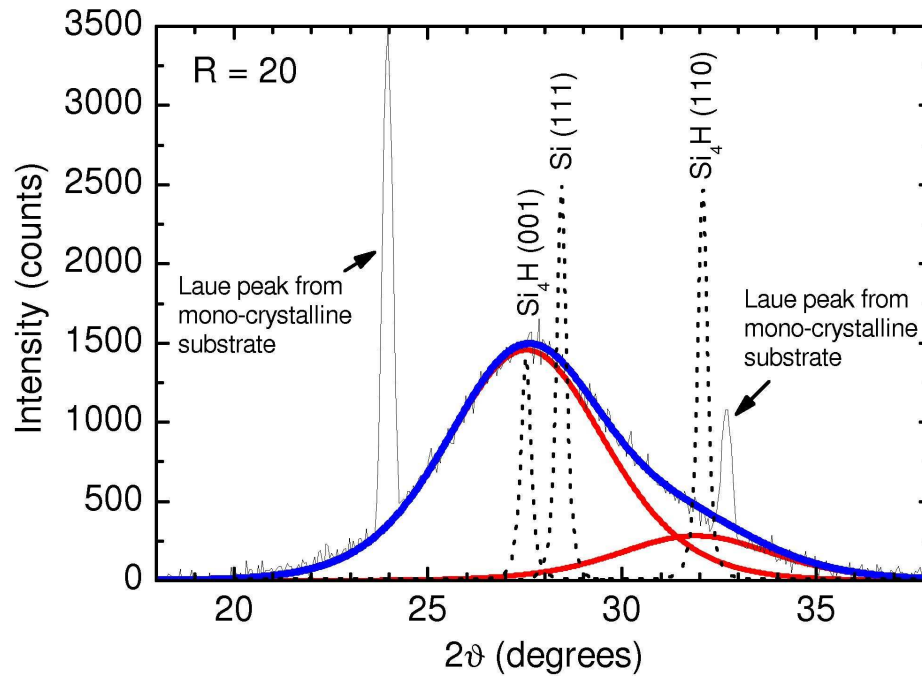


Figure 2: Raw XRD patterns measured on a 300 nm thick film deposited with R=20 on a c-Si substrate.  
90x65mm (600 x 600 DPI)



32  
33  
34  
35  
36  
37  
38  
39  
40  
41  
42  
43  
44  
45  
46  
47  
48  
49  
50  
51  
52  
53  
54  
55  
56  
57  
58  
59  
60

Figure 3: XRD patterns of the FSP after background correction. The peak is fitted with two Pearson VII profiles. Also shown are the XRD lines for crystalline Si and Si<sub>4</sub>H.  
90x65mm (600 x 600 DPI)

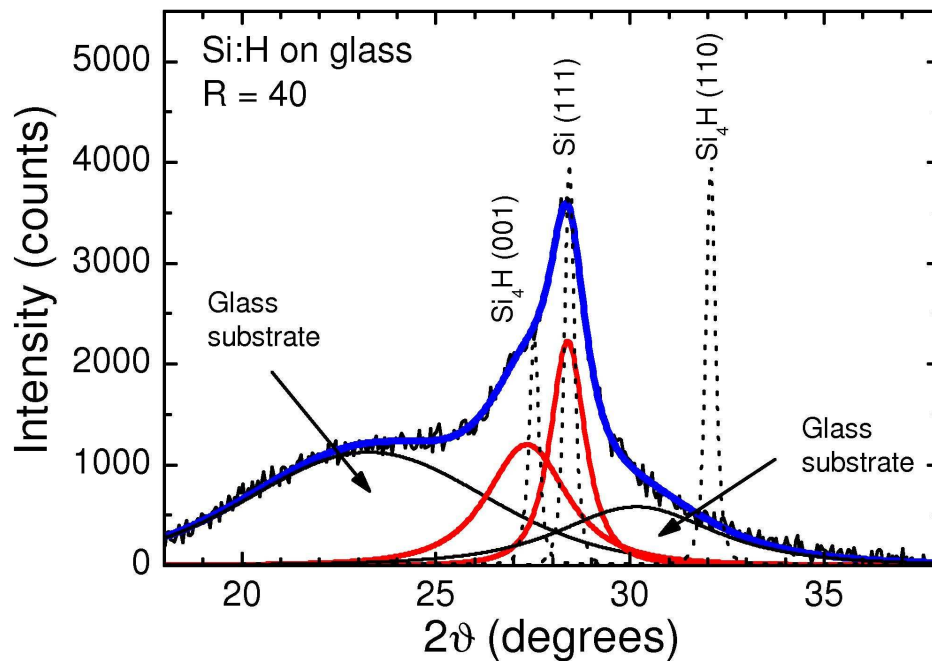
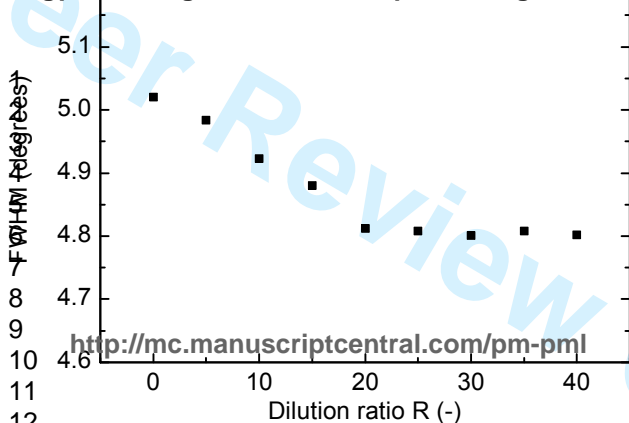


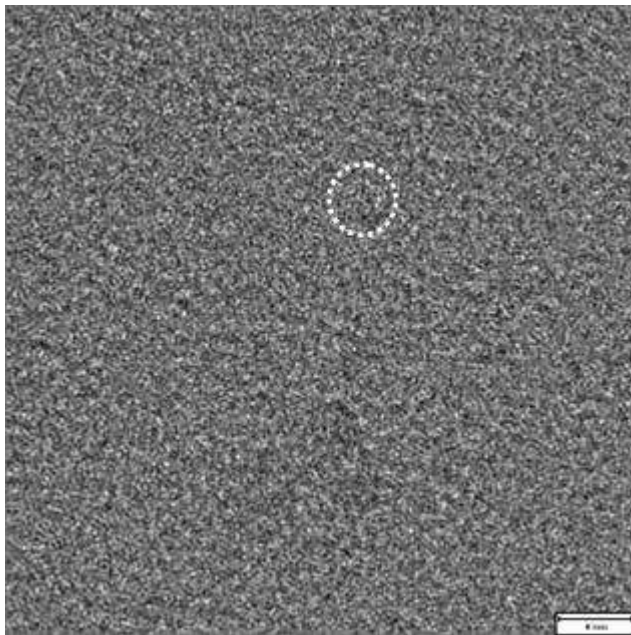
Figure 4: XRD patterns of the FSP after background correction for Si:H film deposited with  $R = 40$  on a glass substrate. Also shown are the XRD lines for crystalline Si and Si<sub>4</sub>H.  
90x65mm (600 x 600 DPI)



<http://mc.manuscriptcentral.com/pm-pml>

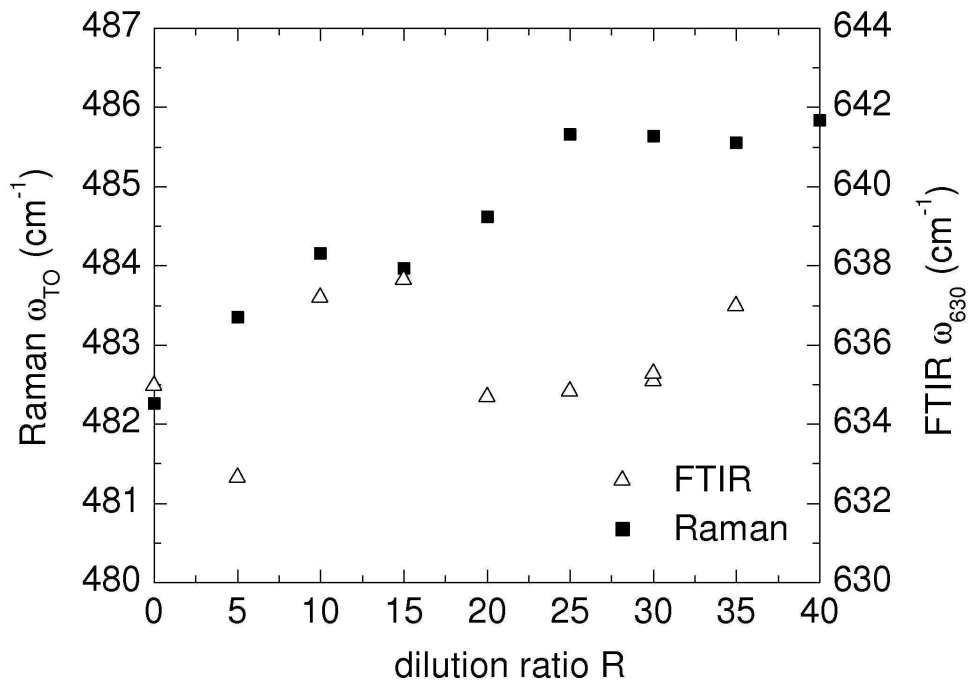
8  
9  
10  
11  
12

1  
2  
3  
4  
5  
6  
7  
8  
9  
10  
11  
12  
13  
14  
15  
16  
17  
18  
19  
20  
21  
22  
23  
24  
25  
26  
27  
28  
29  
30  
31  
32  
33  
34  
35  
36  
37  
38  
39  
40  
41  
42  
43  
44  
45  
46  
47  
48  
49  
50  
51  
52  
53  
54  
55  
56  
57  
58  
59  
60

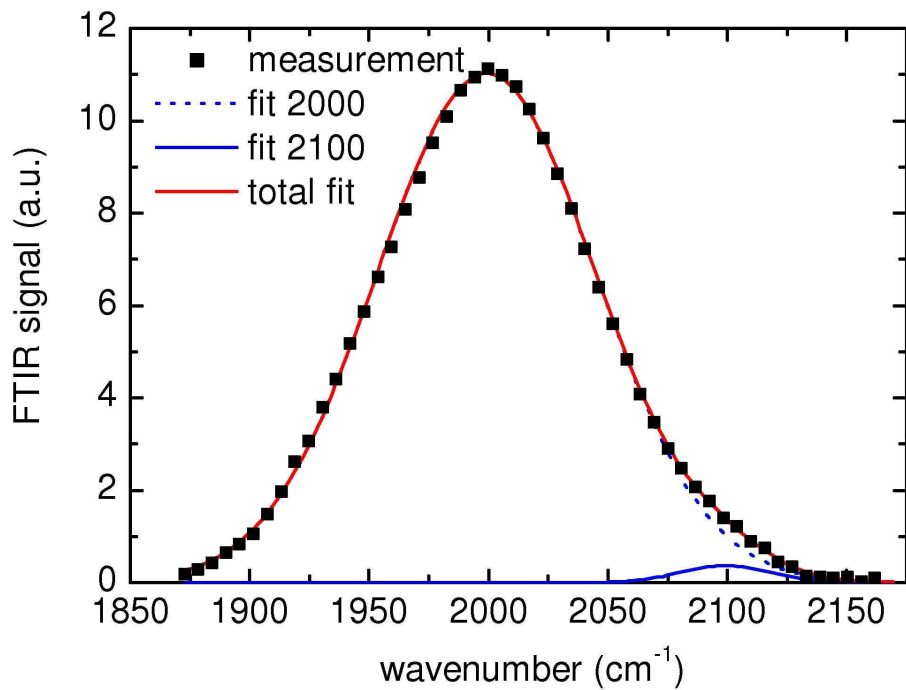


66x66mm (120 x 120 DPI)

Review Only



90x65mm (600 x 600 DPI)



90x65mm (600 x 600 DPI)

View Only

1  
2  
3  
4  
5  
6  
7  
8  
9  
10  
11  
12  
13  
14  
15  
16  
17  
18  
19  
20  
21  
22  
23  
24  
25  
26  
27  
28  
29  
30  
31  
32  
33  
34  
35  
36  
37  
38  
39  
40  
41  
42  
43  
44  
45  
46  
47  
48  
49  
50  
51  
52  
53  
54  
55  
56  
57  
58  
59  
60

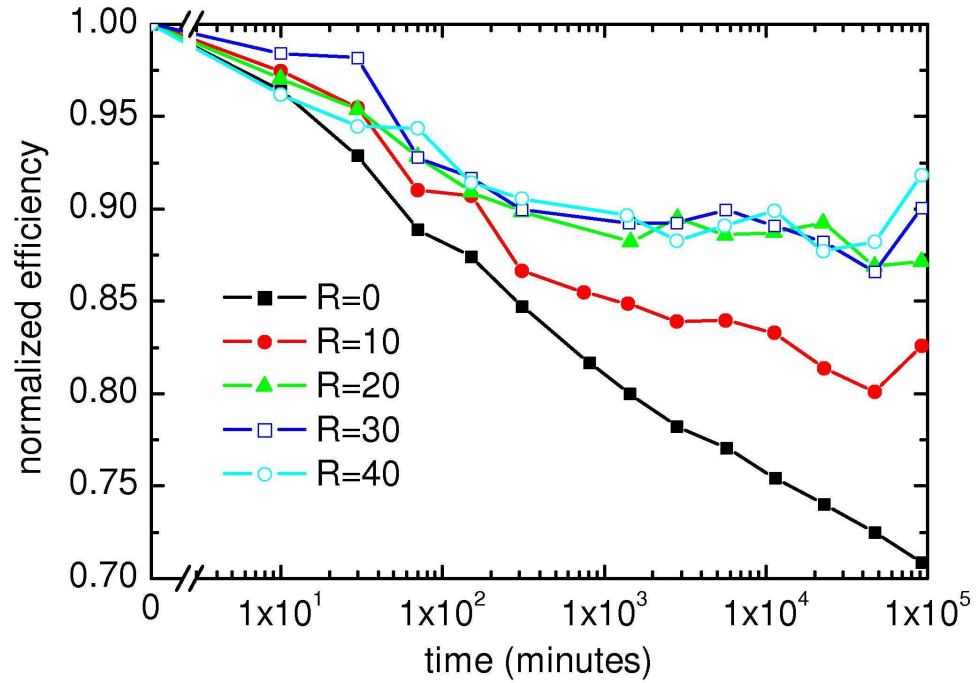


Figure 9: Degradation of the efficiency of solar cells in which the absorber layers have been grown at different R. The data is normalized to the initial efficiency. 90x65mm (600 x 600 DPI)

new Only

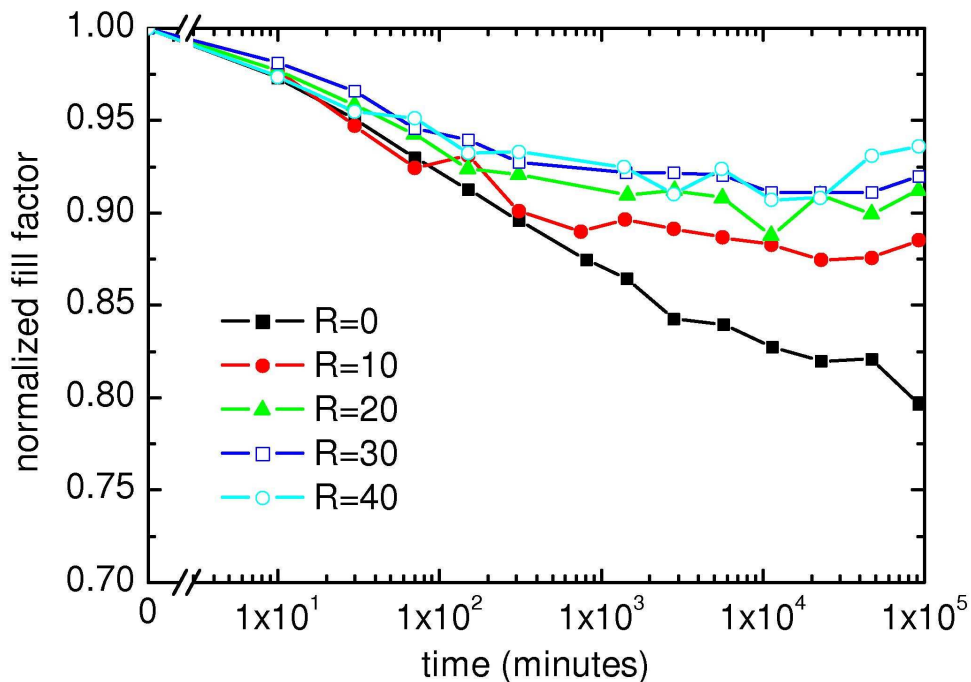


Figure 10: Degradation of the fill factor of solar cells in which the absorber layers have been grown at different R. The data is normalized to the initial fill factor.  
90x65mm (600 x 600 DPI)

new Only